Stationary waves in a nonlinear periodic medium: Strong resonances and localized structures. II. The continuous model

J. Coste and J. Peyraud
Laboratoire de Physique de la Matière Condensée, Université de Nice, Parc Valrose, 06034 Nice CEDEX, France

(Received 21 December 1988; revised manuscript received 6 March 1989)

We study here the stationary waves in a nonlinear medium whose propagation constant is harmonically modulated in space. We recover most of the physical results obtained in the discrete model studied in the preceding paper (part I). However, the bifurcations associated with strong (Arnol'd) resonances exhibit some new features. The problem of "quasi-integrability" of the wave equation near the bifurcations receives special attention. Finally we give some comments on the observability of the stationary localized solutions.

I. INTRODUCTION: THE MODEL AND ITS POINCARÉ MAP

We have considered in the preceding paper (part I) a discrete model in which the refractive index exhibits a δ-like variation on equidistant sites n_i. The advantage of this model was obviously its simplicity. However, it presents some unphysical aspects. In particular the nonlinear Kerr effect was assumed to take place only on sites n_i. It is therefore important to examine if the main features of the stationary solutions obtained in part I survive when the modulation of the refractive index is smooth, and when the Kerr effect acts everywhere.

As in I, the stationary wave equation is considered as a dynamical system whose strong (or Arnol'd) resonances are studied, and the considerations made about the discrete model are unchanged. Near a resonance $k=k_c$, the system is "quasi-integrable," and we delimit the validity of analytical approaches. Roughly speaking we shall say that the convergence of approximate analytic solutions towards exact ones is not uniform. The so-called "gap solitons" of Mills and Trullinger[1] are an example of such approximate solutions which are found in the gaps of the linearized system, and they correspond to one of the four strong resonances. However, we find that this resonant bifurcation also gives rise to kinklike solutions outside the gap (a phenomenon already observed in the discrete model). Kinks and solitons obey, in their analytical approximation, the same "envelope differential equation" of Ref. 1. Since Mills and Trullinger limit their investigation to the interior of the gap, we have been led to reconsider this equation.

The other localized solutions, namely the "triangles" and the "squares" already defined in I as associated with third and fourth strong resonances, are found here with similar characteristics.

Even though small, the stochasticity of the localized solutions induces the same kind of physical effects as in the discrete model, but with greater diversity: one observes random sequences of solitons and kinks, and the critical onset of stochasticity near a bifurcation is characterized by a new critical exponent when two pairs of fixed points are issued from the bifurcation (double bifurcation).

The paper is organized as follows. In Sec. II we consider two limiting systems, which help to understand the physical origin of the observed bifurcations. In Sec. III the fourth resonances are successively analyzed. In Secs. IV and V we study the stochastic behavior and the physical observability of the localized solutions.

We assume that the modulation of the refractive index is harmonic and has the form $n=n_0(1+\mu|\Psi|^2)[1+\varepsilon\cos(2x)]$. Looking for a solution of the time-dependent wave equation of the form $\Phi(x,t)=\Psi(x)e^{i\omega t}+\text{c.c.}$ (with $\omega=kc$), we obtain that Ψ obeys the equation

$$\{\partial_x^2+k^2(1+\mu|\Psi|^2)[1+\varepsilon\cos(2x)]\}\Psi=0\ , \tag{1}$$

where k is the wave number in the unmodulated medium. There is only a minor difference between Eq. (1) and the wave equation considered by Mills and Trullinger, namely the presence in the former of the term proportional to $\mu\varepsilon$: this term would not give any additional contribution to the "envelope equation" of Ref. 1.

Showing that Ψ can be taken real when zero flux propagation is considered follows from an argument similar to those used in the discrete case. Since localized solutions are necessarily of the zero-flux type (see I), we consider only this case in the present paper. Setting

$$y=\Psi\sqrt{\mu}\ , \tag{2}$$

Eq. (1) reads

$$\{\partial_x^2+k^2(1+\eta y^2)[1+\varepsilon\cos(2x)]\}y=0\ , \tag{3}$$

where $\eta=\text{sgn}(\mu)$.

Like the mapping describing the discrete model, Eq. (3) does not depend on $|\mu|$.

It is convenient to associate with Eq. (3) the Poincaré map G defined as follows:

$$\begin{Bmatrix} y(x) \\ y'(x) \end{Bmatrix} \xrightarrow{G} \begin{Bmatrix} y(x+\pi) \\ y'(x+\pi) \end{Bmatrix}, \quad \text{with } y' = \frac{dy}{dx} \tag{4}$$

(remember that π is the period of the refractive index modulation). Actually we shall take our initial values at $x=0$, and put

$$X_j = y(j\pi), \quad Y_j = y'(j\pi) , \tag{5}$$

making G a mapping of the (X, Y) plane into itself.

Before entering the subject of strong resonances, it is interesting to relate the fixed points of G and $G^{(2)}$ to those of known limiting integrable systems.

II. FIXED POINTS OF G AND $G^{(2)}$ AND LIMITING INTEGRABLE SYSTEMS

The fixed points of G and $G^{(2)}$ are the periodic solutions of Eq. (3) with period 2π and π, respectively. Before determining them, it is interesting to observe that our dynamical system is well known in the two following limits.

(i) $\mu=0$: it is the linear limit and the system is then described by the Mathieu equation

$$\{\partial_x^2 + k^2[1+\varepsilon\cos(2x)]\}y = 0 . \tag{6}$$

The solutions are of the Floquet type and are either propagative in passing bands or damped in the gaps. The gaps of the Mathieu equation are located in the neighborhood of $k=n$ and their size is a rapidly decreasing function of n. This makes a noticeable difference with the case of the discrete model. On the edges of the nth gap the solutions are exactly periodic with period $2\pi/n$. These solutions yield fixed points of $G^{(2)}$ for $n=1$ (first gap) and of G for $n=2$ (second gap).

(ii) $\varepsilon=0$: nonlinear unmodulated system (UMS), governed by the equation

$$[\partial_x^2 + k^2(1+\mu y^2)]y = 0 . \tag{7}$$

Equation (7) is integrable and it describes, if x has the meaning of a time variable, the motion of a particle in the potential

$$V(y) = k^2(y^2/2 + \mu y^4/4) .$$

The solutions are periodic for $\mu>0$ and for $\mu<0$ [provided that $y<(-2/\mu)^{1/2}$], the nonlinearity simply making the oscillation anharmonic. The oscillation period is a monotonic function of the amplitude (growing or decreasing according to the sign of μ). Therefore there exist periodic solutions with period $2\pi/n$ in the vicinity of $k=n$. Moreover, these solutions, which have definite amplitudes for given k, are stable, and they correspond to elliptic fixed points of G and $G^{(2)}$. They exist whatever the sign of the Kerr constant.

These two types of solutions survive, as we shall see, in the original system; that is, for ε and μ different from zero. In particular the elliptic fixed points of G and $G^{(2)}$ will always exist, whatever the sign of μ. This is also an important difference with respect to the discrete model.

III. STRONG RESONANCES AND LOCALIZED STATES

As in the case of the discrete model, the continuous dynamical system is "nearly integrable" in a small neighborhood of the elliptic periodic points of the mapping, and the considerations we have developed in I concerning the strong resonances of the dynamical system remain unchanged. In particular, the strong resonances are associated with the bifurcation at the origin of cycles of G with winding number $\varphi/2\pi = 1/n$ ($n=1,2,3,4$), where φ is the phase shift experienced by the wave, in a stationary solution, over a modulation period. In terms of the continuous flow, a solution corresponding to one of these strong resonances has the form

$$y(x) = Z(x)e^{ik_1 x} \tag{8}$$

with $\varphi = k_1\pi/2\pi = k_1/2$. $Z(x)$ is a slowly varying complex function; that is, its characteristic length of variation λ^{-1} is much larger than k_1^{-1}. As we shall see below, the complex function $Z(\lambda x)$ will be approximated, near a bifurcation, by the solution of a first-order differential equation. Note that $y(nj\pi)$ and $y'(nj\pi)$ are equal to $2\,\mathrm{Re}[Z(nj\pi)]$ and $-2k_1\,\mathrm{Im}[Z(nj\pi)]$, respectively. Therefore the orbit points of $G^{(n)}$ belong to the continuous curve in the (X, Y) plane defined by $X = 2\,\mathrm{Re}[Z(x)]$, and $Y = -2k_1\,\mathrm{Im}[Z(x)]$. Moreover $\lambda \ll k_1$ implies that successive orbit points are very close to each other. Therefore the existence of solutions of the form (8) implies that, near a bifurcation, mapping $G^{(n)}$ can be approximated, in an appropriate sense, by a set of two real, first-order differential equations, as was the case in the discrete model. Then our original dynamical system $[O]$ has been replaced by an integrable one $[R]$. What is meant by "an approximate sense"? We know that the neighborhood of the hyperbolic points of $[O]$ remains chaotic, even though the size of the stochastic domains may be quite small. As a result the orbit solutions of $[O]$ and $[R]$ are expected to be close to each other only over finite x intervals. They diverge at long distances. Moreover, we know from the study of the discrete model that "quasi-integrability" holds only near the bifurcation values of the control parameters, and when one looks for orbit solutions close to the bifurcated points. These observations must be kept in mind when analytic solutions, obtained with the help of perturbative methods, will be compared with exact solutions.

Now these analytic solutions are conveniently analyzed in the frame of Poincaré-Lindset perturbation theory (which is equivalent to the method of normal forms used in I). The details of the calculations are available in the appendixes.

The first two strong resonances ($n=1,2$) correspond respectively to $k_1=2$ (first linear gap) and $k_1=1$ (second gap). Let us first observe that the continuous model irreducibly depends on the two parameters k and ε, instead of the unique parameter E_0 of the discrete model. In view of the above considerations we are looking for a solution near a bifurcation value $k=k_c$ associated with a strong resonance. Therefore it would seem natural to organize a perturbative calculation in the following way:

first find an ε expansion of the exact Floquet solution $F_1(x)$ of the linearized system for $k=k_c$; second, use $F_1(x)$ as the zeroth-order solution of the nonlinear wave equation, with respect to expansion parameter $\lambda^2=k^2-k_c^2$. This program is indeed applicable to the calculation of the third and fourth resonances because the origin is then a regular point of the linear system. In the case of the two first resonances, the origin changes its stability at the bifurcation value, and, as a result, $F_1(x)$ must itself be expanded in terms of the two parameters ε and λ. Then it proves appropriate to use the same perturbative method for solving the nonlinear equation as those already needed for solving the Floquet problem.

A. Second resonance: First gap ($k\approx 1$)

This gap is defined by $k^2\in[1-\varepsilon/2,1+\varepsilon/2]$. Setting $\delta k^2=k^2-1$, we look for a solution of the form

$$y(x)=Z(x)e^{ix}+\text{c.c.} \tag{9}$$

The perturbative calculation (see Appendix A) uses ε as the expansion parameter and starts at the lowest order from the solution of the linear, unmodulated equation. One finds at second perturbative order the following solvability condition:

$$2i\partial_x Z+(\delta k^2+3\eta|Z|^2)Z+\frac{\varepsilon}{2}Z^*=0\ . \tag{10}$$

As could be expected, Eq. (10) and its complex conjugate are nothing but the "envelope equations" of Mills and Trullinger. These equations define an integrable system.

A first remark is that in the variable change $\{\delta k^2\to-(\delta k^2),\ \eta\to-\eta,\ Z\to iZ^*\}$ Eq. (10) is transformed to its complex conjugate. In other words, changing η to $-\eta$ and δk^2 to $-(\delta k^2)$, an orbit solution is changed to its symmetric reflection about the first bissectrix. Therefore we can limit ourselves to study of the case $\eta=1$.

The fixed points of $G^{(2)}$ correspond to 2π-periodic solutions of Eq. (3); that is, to x-independent solutions of Eq. (10). One obtains two such solutions:

$$y_{\rm I}=\pm\Lambda_{\rm I}\sin x \quad \text{with } \Lambda_{\rm I}=\left[\frac{4}{3}\eta\left[1+\frac{\varepsilon}{2}-k^2\right]\right]^{1/2} \tag{11}$$

and

$$y_{\rm II}=\pm\Lambda_{\rm II}\cos x \quad \text{with } \Lambda_{\rm II}=\left[\frac{4}{3}\eta\left[1-\frac{\varepsilon}{2}-k^2\right]\right]^{1/2}\ . \tag{12}$$

It is worth remarking that the determination of the fixed points of the mapping by perturbation theory does not suffer the above-mentioned restrictions concerning the determination of the heteroclinic orbits. Solutions $y_{\rm I}$ are stable (see Appendix A) and reminiscent of the UMS solutions. They provide two elliptic points $F(0,\Lambda_{\rm I})$ and $F'(0,-\Lambda_{\rm I})$ of $G^{(2)}$ located on the Y axis. Solutions $y_{\rm II}$ yield two hyperbolic fixed points $H(0,\Lambda_{\rm II})$ and $H'(0,-\Lambda_{\rm II})$ of $G^{(2)}$ located on the X axis, and correspond to the periodic Floquet solutions of the Mathieu equation. These results permit one to obtain the bifurcation diagrams represented in Figs. 1(a) and 1(b) for $\eta=1$ and $\eta=-1$, respectively. The above bifurcations present some differences with those observed in the discrete model. First, two bifurcated solutions appear instead of one, when crossing a gap in the appropriate sense (compare with the bifurcation diagrams of the discrete model). Second, in the case where hyperbolic and elliptic fixed points coexist, the former are located at a finite distance from the origin in the discrete model, while they are close to the origin in the continuous model since they bifurcate from one of the gap edges.

1. Solutions inside the gap

Instead of looking directly for a complex solution $Z(x)$ of Eq. (10), as in Ref. 1, it proves much simpler to first determine an orbit solution in the (X,Y) plane. Remember that the orbit points are located on the continuous curves defined here by $X=2\,\mathrm{Re}(Z)$, $Y=-2\,\mathrm{Im}(Z)$. Set

$$2Z=\rho e^{i\theta}\ ,$$

ρ and $-\theta$ being the modulus and the argument of complex number (X,Y). From Eq. (10) ρ and θ obey the equations

$$\frac{d\rho}{dx}=\frac{\varepsilon}{4}\rho\sin(2\theta)\ , \tag{13}$$

$$2\frac{d\theta}{dx}=\delta k^2+\frac{3\rho^2}{4}+\frac{\varepsilon}{2}\cos(2\theta)\ . \tag{14}$$

From these equations we deduce the differential equation obeyed by the orbit:

$$\frac{dT}{d\theta}=\frac{\varepsilon T\sin(2\theta)}{\delta k^2+3T+\frac{1}{2}\varepsilon\cos(2\theta)}\ ,$$

where $T=\rho^2/4$. This equation is easily integrated, yielding the solution

$$3T^2+[2\delta k^2+\varepsilon\cos(2\theta)]T=K\ , \tag{15}$$

where K is an arbitrary constant. Inside the gap the separatrix (homoclinic orbit of the origin) corresponds to $K=0$, and its equation is

$$3\rho^2=-4[2\delta k^2+\varepsilon\cos(2\theta)]\ . \tag{16}$$

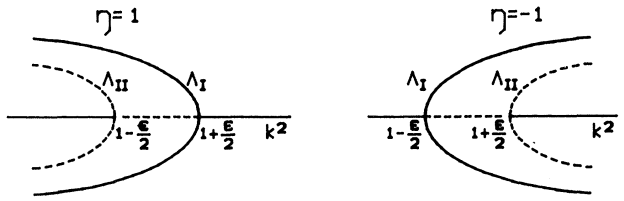

FIG. 1. Bifurcation diagrams in the first gap ($k\approx 1$). (a) $\eta=1$; (b) $\eta=-1$.

Then solving Eq. (14) gives

$$\tan\theta = -\left[\frac{1+b}{1-b}\right]^{1/2}\frac{1+e^{-ax}}{1-e^{-ax}}\ , \tag{17}$$

where $b=2\delta k^2/\varepsilon$ and $a=\varepsilon(1-b^2)^{1/2}/2$. Equations (14) and (15) are of course consistent with analytic expressions of the solitonic solution given in Ref. 1. We remark in particular that the orbit solution at the midgap ($\delta k^2=0$) takes the form of a Bernouilli lemniscate.

2. *Solutions outside the gap*

The solutions outside the gap have not been studied by Mills and Trullinger. The heteroclinic orbits (passing through points H and H') corresponds to $K=-\lambda^2/4$. Setting

$$\lambda^2 = -\varepsilon/2-\delta k^2 = k_c^2-k^2\ ,$$

($k_c^2=1-\varepsilon/2$ is the bifurcation value of the hyperbolic fixed points), the equation of these orbits reads

$$\tfrac{3}{4}\rho^2 = \lambda^2+\varepsilon\sin^2\theta \pm \varepsilon|\sin\theta|(\sin^2\theta+g^2)^{1/2} \tag{18}$$

with $g^2=2\lambda^2/\varepsilon$. Then solving Eq. (14) gives

$$\ln\left[\frac{(g^2+\sin^2\theta)^{1/2}-g\cos\theta}{(g^2+\sin^2\theta)^{1/2}+g\cos\theta}\right] = \pm\varepsilon\mu x\ . \tag{19}$$

Equation (18) is the polar representation of two curves in the (X, Y) plane (see Fig. 2).

(i) C_1, which corresponds to the minus sign in Eq. (18), is the shortest path connecting H and H'. It represents a kinklike solution.

(ii) C_2, which corresponds to plus sign in Eq. (18), circles around F and F'. In the limit of small λ this orbit is very similar to the solitonic orbits found inside the gap. Therefore we shall call "solitonlike" the part of an orbit which is close to (C_2).

Note that the term "kink" was used in Ref. 1 to characterize the spatial variation of the soliton phase. Here the kinks are localized structures whose amplitude is nearly constant, except near isolated points where it falls. They correspond to the "dark solitons" of the theory of nonlinear dispersive media.

On the left boundary of the gap ($\lambda=0$), Eq. (18), taken with the plus sign, shows that the orbit solutions consist of two circles centered on the Y axis and tangent to each other at origin. Their equation is

$$X^2+[Y\pm(2\varepsilon/3)^{1/2}]^2 = 2\varepsilon/3\ .$$

Phase portraits of homoclinic and heteroclinic orbits inside and outside the first gap are shown in Fig. 2.

Several remarks are in order.

(a) In the above solutions the field sign changes on two consecutive space points distant by π (the modulation period). Indeed, successive orbit points in the phase space of G would belong alternately to the upper and lower half-planes. Therefore the solitonic orbits are of the "alternate type," according to the terminology used in I.

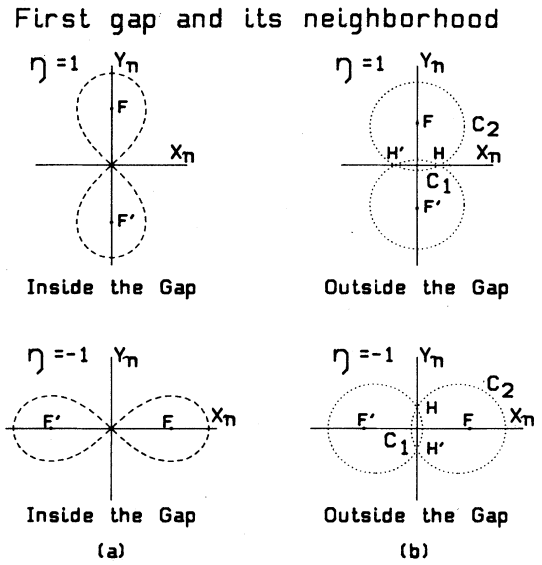

FIG. 2. Schematical phase portraits of the continuous model for $\eta=\pm1$. (a), inside the first gap: F and F' are the elliptic fixed points of the Poincaré map $G^{(2)}$. (b), outside the gap: in addition to F and F' there appear the hyperbolic fixed points H and H'.

(b) On the left side of the gap, we expect three types of orbit solutions which are close either to C_1 or to C_2.

(i) Kinklike orbits located inside C_1.

(ii) "Kink solitons": the orbit first follows C_1 from H to H', then follows C_2 (around F or F'), terminating back at H.

(iii) "Double solitons": the orbit starting at H follows C_2 first around F' then around F.

Actually we shall see that these various types of solutions are "connected" to each other by the stochasticity.

3. *Peak width of the localized solutions*

For $\eta=1$ the solitonlike solutions are created on the right edge k_c of the gap ($k_c^2=1+\varepsilon/2$). When $k\to k_c$ Eqs. (16) and (17) show that the peak amplitude of the soliton decreases like λ ($\lambda^2=k_c^2-k^2$), while the peak profile decreases with respect to x like e^{-ax} ($a=\lambda\sqrt{\varepsilon/2}$). As a result the peak width is proportional to $(\lambda\sqrt{\varepsilon})^{-1}$.

Things are somewhat more complicated on the left edge of the gap ($k_c^2=1-\varepsilon/2$). Indeed two types of behavior are expected in terms of the value of parameter g entering Eq. (19).

(i) If $g>1$ (or $\lambda<\sqrt{\varepsilon/2}$), then either the soliton or kinklike orbit solution approaches fixed point H or H' exponentially. More precisely, if we set $\rho_h=|OH|$, we find that for large x, θ and $\rho^2-\rho_h^2$ are proportional to $e^{-\varepsilon g x/2}$.

As a result the characteristic peak width of the two types of solutions is again proportional to $(\lambda\sqrt{\varepsilon})^{-1}$.

(ii) If $g \ll 1$, then the decay of the localized structure proceeds along two successive stages.

First. A preasymptotic regime in which $\sin\theta \gg g$. Then $\tan\theta \approx -2/\varepsilon x$ and $\rho^2-\rho_h^2$ is either nearly constant and equal to $-\varepsilon g^2$ (the case of the kinklike solution), or decreases like $-8/\varepsilon x^2$ (the case of the solitonlike solution).

Second. The full asymptotic regime in which $\sin\theta \ll g$. It is characterized by the same exponential decay as in case (i). The passage from the first to the second regime takes place at an x value of the order of $(\lambda\sqrt{\varepsilon})^{-1}$.

At an exact bifurcation value ($\lambda=0$) the second stage disappears and the solitonic solution decays like $-8/\varepsilon x^2$; that is, very slowly. One finds that the minimum width of the soliton peak is obtained at the midgap. Summarizing, the soliton near the right edge of the gap and the kink on the left edge have similar overall characteristics (peak amplitude and spatial decay). This is natural since one considers these two solutions near their bifurcation. On the contrary, the solitonic solution near the left edge of the gap has not only a finite amplitude for given ε, but it also decays differently.

Now the above analytic solutions are exact only if k is close to a bifurcation value k_c. Therefore we expect that the solitons exhibit more and more chaotic behavior as one moves from the right to the left edge of the gap. This is confirmed by numerical results.

3. *Exact solutions from numerical integration*

We present two typical phase portraits of $G^{(2)}$ obtained numerically inside and outside the gap.

Figure 3(a) is a phase portrait of mapping $G^{(2)}$ inside the gap, showing a solitonlike solution, with an enlarged portion of it around the origin, and Fig. 3(b) shows the graph of $(-1)^n X_n$, which exhibits multiple peaks with random signs and weakly random amplitudes. In an integrable system the peak signs would be all the same. Here the solution "hesitates" at each passage near the origin between two possibilities: stay in the same half (X, Y) plane, or get to the other one.

Figures 4(a) and 4(b) show the phase portrait on the left side of the gap. We see a stochastic orbit which can be looked at as the union of a kinklike and a solitonic part. In Fig. 4(c) we show the graph of $\log_{10}(|X_n|^2+|Y_n|^2)$, which exhibits a typical random alternation of kinks and solitons. Again the solution hesitates at each passage near H or H' between two possibilities: follow C_1 or C_2. As a result one obtains random sequences of the three above-mentioned types of orbits.

B. First resonance (second gap: $k \approx 2$)

This gap is defined by $k^2 \in [1+5\varepsilon^2/3, 1-\varepsilon^2/3]$. The solution with correctly scaled variables has the form

$$y(x)=Z(x)e^{2ix}+\text{c.c.} ,$$

where Z is a function of $\lambda^2 x$ (see Appendix A). Then the

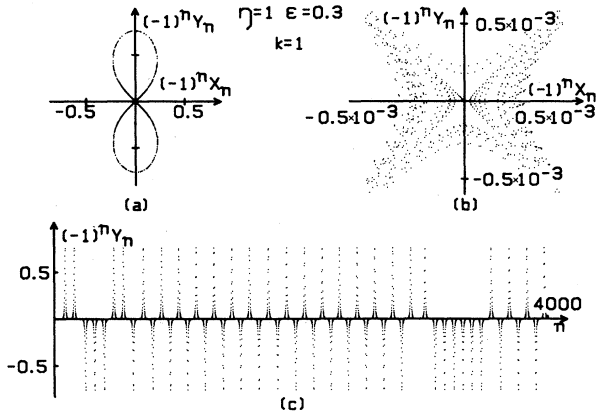

FIG. 3. Random sequences of gap solitons inside the first gap ($\eta=1$). (a) Global phase portrait of $G^{(2)}$. (b) Detailed phase portrait near the origin. (c) Graph of $(-1)^n X_n$ as a function of n.

following solvability condition is obtained at third perturbative order:

$$4i\partial_x Z+\left[\delta k^2-\frac{2\varepsilon^2}{3}+12\eta|Z|^2\right]Z-Z^*=0 . \qquad (20)$$

Here $\delta k^2=k^2-4$ (δk^2 is of the order of ε^2).

The fixed points of G correspond to π-periodic solutions of Eq. (3) in the neighborhood of $k=2$ (second gap). They are determined in Appendix A and they read

$$y_{\mathrm{I}}=\pm\left[\frac{\eta}{3}(4+\tfrac{5}{3}\varepsilon^2-k^2)\right]^{1/2}\cos(2x) ,$$

$$y_{\mathrm{II}}=\pm\left[\frac{\eta}{3}(4-\tfrac{1}{3}\varepsilon^2-k^2)\right]^{1/2}\sin(2x) .$$

The bifurcation diagrams in the neighborhood of the

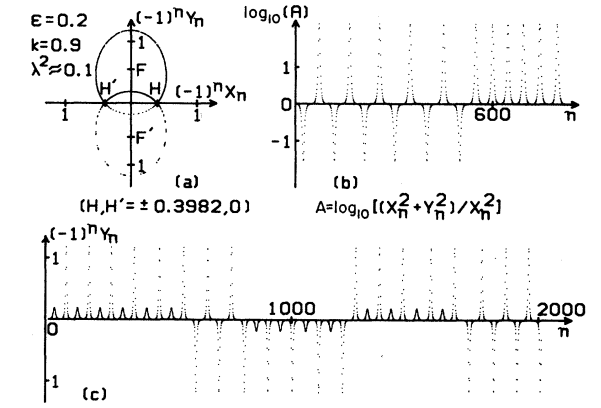

FIG. 4. Random sequences of solitons and kinks on the left side of the first gap. (a) Global phase portrait of $G^{(2)}$. (b) Detailed phase portrait near the origin. (c) Graph of $\log_{10}(|X_n^2|+|Y_n^2|)$ as a function of n.

second gap are quite analogous to those found in the first one. The only differences are the following.

(i) The size of the second gap is of order ε^2 instead of ε.

(ii) The elliptic and hyperbolic fixed points are found, respectively (for $\eta=1$), on the X and on the Y axis.

(iii) The solitonic orbits are of the nonalternate type.

C. The fourth resonance ($k \approx \frac{1}{2}$)

We give in Appendix B a detailed analysis of the fourth resonance, which takes place at $k=\frac{1}{2}$; that is, in the first passing band. The main lines of the calculation are the following. The unperturbed state of the Poincaré-Lindset expansion is now the exact Floquet solution of the linear system and the perturbation parameter of the theory is no longer ε but λ (the deviation of k from its bifurcation value), ε being looked at as finite.

The orbits are similar to those found in the discrete model. In particular, the heteroclinic orbits are two entangled ellipses whose equations are

$$X^2/4+Y^2\pm\sqrt{\varepsilon}XY=4\lambda^2/3\ . \tag{21}$$

The difference with the discrete case is that here, the relative size of the elliptical domains around the elliptic points (which is a measure of the "amplitude" of the resonance) is of the order of $\sqrt{\varepsilon}$ (instead of being ε independent) and therefore goes to zero when $\varepsilon\to 0$.

Figure 5 shows a period-4 cycle inside the first pass band.

D. Third resonance

As in the discrete model, the bifurcation at the origin of the periodic solution with $k_1=\frac{2}{3}$ is a weak resonance, because of the absence of quadratic terms in the wave equation. Therefore a strong third resonance can be obtained only as a secondary bifurcation; for example, as the bifurcation of the elliptic points of the period-4 cycle of the origin. But the determination of these points cannot be made using a perturbative method, because they are at a finite distance from the origin when they bifurcate towards a period-3 cycle. Therefore, this bifurcation has been determined numerically. We have again obtained a heteroclinic orbit of triangular form, and the triangle (whose size is proportional to λ) preserves its form when $\lambda\to 0$. As in the discrete model, it is surrounded by a strongly stochastic domain. Figure 6 shows such a period-3 cycle.

Note also that there does not exist a period-3 cycle bifurcated from an elliptic point of G through a strong resonance process. This bifurcation is ruled out by the symmetry properties of the model.

We have not represented in Figs. 5 and 6 the spatial variation of the phase and of the amplitude of the solution, since they are quite similar to those obtained in the discrete model.

IV. STOCHASTIC BEHAVIOR OF THE LOCALIZED SOLUTIONS

As in the discrete model the orbits are found to be chaotic, even near the bifurcation points. However, giving direct numerical evidence of the stochasticity is more difficult than in the previous model. Indeed, numerical integration consists in replacing the original continuous equation by a discrete mapping, and it is well known that one easily introduces in this way nonanalytic behaviors which do not belong to the original model. Moreover, great accuracy is needed for determining an orbit (assumed truly chaotic), because such an orbit is sensitive to initial conditions. Therefore one must estimate and control the precision of the employed numerical algorithm (here it is an x-dependent Runge-Kutta procedure), and verify that the orbit points are independent of the length of the integration step, provided it is small enough. We have been led to use up to 12 000 iterations per modulation period, and to perform the calculations with 19-digit numbers.

The stochasticity disappears when $\varepsilon\to 0$ whatever the values of k, since we know that the wave equation is integrable in this limit. But, for finite ε, numerical integration confirms that it also disappears at bifurcation values, as in the discrete model.

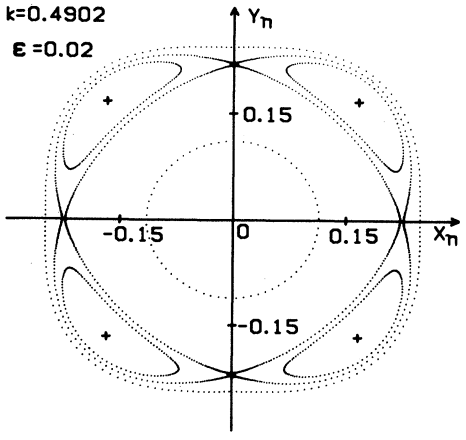

FIG. 5. Phase portrait of a period-4 cycle.

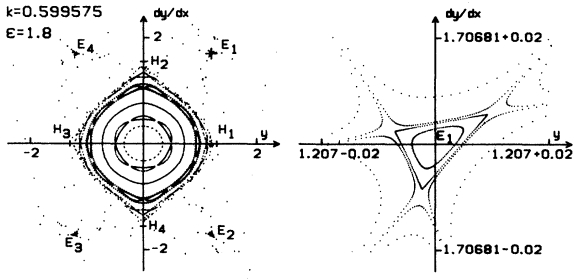

FIG. 6. Phase portrait of a period-3 cycle bifurcated from the elliptic points of a period-4 cycle. We have chosen this large value of ε in order to obtain a readable figure. But this cycle exists also in the pass band for a small ε value. Points E_i and H_i, respectively represent the elliptic and hyperbolic points of the period-4 cycle.

We have already seen that the stochasticity is responsible for the existence of random sequences of solitons (with random signs of the peak amplitude) and kinks. It also imposes, as in the discrete model, a maximum spatial extension to the localized structures. To study this phenomenon, we shall follow exactly the same lines as in the discrete model, and we shall consider the case of a solitonic solution. Then, being given an initial point in the (X, Y) plane located on the Y axis, whose distance from the origin is δ, δ' is the minimal distance to the origin of a first-return orbit point. The graph of δ' as a function of δ exhibits again a sharp transition to a stochastic regime at a well-defined value δ_c. The variation of $\log_{10}(1/\delta_c)$ with k^2 is represented on Fig. 7(b) for a given value of ε. We observe that the variation is monotonic all along the gap. $1/\delta_c$ diverges when $k \to k_+$, the upper gap edge, while it goes to a finite value on the lower edge k_-. This confirms the fact that the stochasticity of the solitonlike solutions increases from the upper to the lower gap edge; that is, when one departs from the bifurcation which gives rise to the solitonic solution. Now, at $k = k_-$, $\log_{10}(1/\delta_c)$ is a growing function of ε which vanishes when $\varepsilon \to 0$. We therefore conclude that analytic behavior is expected for any solution in the gap only in the limit $\varepsilon \to 0$ (but this solution has a vanishingly small amplitude).

λ being defined as $\lambda^2 = |k_+^2 - k^2|$, we find that, when $k \to k_+$, $\log_{10}(1/\delta_c)$ diverges like $\lambda^{-\nu}$ with $\nu \approx 1.4$: this critical exponent seems to be the same as those found in the discrete model. We also observe the same detailed structure of the curve $\log_{10}(1/\delta_c)$ as a function of k^2, namely a set of plateaus with decreasing amplitudes when $\lambda \to 0$. We have not determined the critical exponent on the left side of the gap (onset of the kinklike solution) but it is most likely the same.

On the other hand, a different critical exponent is expected at parameter values $\{k = 1, \varepsilon = 0\}$ where the two bifurcations (giving rise to elliptic and hyperbolic fixed points, respectively) take place at the same time (double bifurcation); see Fig. 7(a). Indeed, we find in this case $\nu \approx 2.5$.

Now δ_c is obtained after N_c mapping iterations. Therefore N_c is a measure of the spatial extension of the soliton (using as unit length the modulation period). N_c is found to be proportional to $\log_{10}(1/\delta_c)$: this is not surprising since $\delta_c e^{\gamma N_c} \simeq \lambda$, the fixed point amplitude (γ being the Floquet exponent of the origin). Therefore $N_c \simeq \log_{10}\lambda + \log_{10}(1/\delta_c) \approx \log_{10}(1/\delta_c)$, since $\log_{10}(1/\delta_c)$ diverges as $\lambda^{-\nu}$.

Finally, it is interesting to remark that, being given a localized solution (kink or soliton), it may be characterized by two length scales. (i) the peak width l_p. When $k \to k_c$ (the bifurcation value), l_p diverges like λ^{-1}. (ii) The maximum spatial extent (MSE) of the soliton. This quantity, introduced in I, is the maximum interpeak distance in a multipeak solution, or the maximum length of a system supporting a one-peak solution. MSE is due to the stochasticity of the origin neighborhood, and it is measured by N_c. One may also define the "relative spatial extent" of the soliton as $l_p/(\Delta x)_{\mathrm{MSE}}$, which goes to zero like $\lambda^{\nu-1}$ when $k \to k_c$. In the case of a solitonic solution near the lower gap edge (for $\eta = 1$), the stochasticity is determined by ε instead of λ. Moreover, the peak profile decreases like $1/x^2$. Therefore the notion of relative spatial extension loses its meaning.

V. OBSERVABILITY OF THE LOCALIZED SOLUTIONS

We have indicated that the localized solutions are necessarily of the zero-flux type. This zero-flux condition can be physically realized in several ways. We shall comment on two of them.

(1) Consider a system (finite propagative medium) which is illuminated from both sides with equal wave intensities and let us assume that the wave number falls inside the first gap. In order to correctly express the boundary conditions, we split the amplitude of the sta-

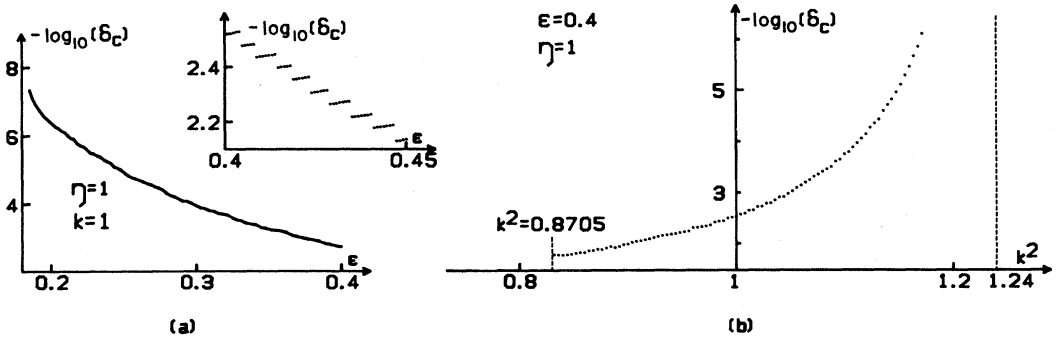

FIG. 7. Variation of $\log_{10}(1/\delta_c)$ in two cases. (a) $k = 1$ (midgap), ε variable. $\varepsilon = 0$ corresponds to the double bifurcation (generation of two pairs of fixed points of $G^{(2)}$). The figure represents the graph of $\log(1/\delta_c)$ as a function of ε. (b) ε fixed ($\varepsilon = 0.4$), k variable. It is the case of a simple bifurcation (creation of the elliptic fixed points), taking place at $k_+^2 = 1.24$ (upper gap edge). The lower edge of the gap corresponds to $k_-^2 = 0.8705$. The figure represents the graph of the $\log_{10}(1/\delta_c)$ as a function of k^2. In the two cases the detailed structure of the graph is a set of nearly horizontal plateaus connected by sharp discontinuities as in the discrete model. This structure is apparent on an enlargement of a portion of the first graph.

tionary wave outside the nonlinear medium, into its two components propagating right and left (see Fig. 8):

$$\Psi(x)=E^{+}e^{ikx}+E^{-}e^{-ikx} \quad [\text{with } E^{-}=(E^{+})^{*}] ,$$

$$\Psi'(x)=ik(E^{+}e^{ikx}-E^{-}e^{-ikx}) .$$

Since we assumed that $|E_0^+|=|E_f^-|$, we can write

$$E_0^+=\frac{|E_0|}{2}e^{-i\varphi}, \quad E_0^-=\frac{|E_0|}{2}e^{i\varphi} ,$$

where 2φ is the phase shift between E_0^+ and E_f^-. These relations read, in terms of $\Psi(0)$ and $\Psi'(0)$,

$$\Psi(0)=|E_0|\cos\varphi, \quad \Psi'(0)=k|E_0|\sin\varphi .$$

As a result, the initial point a_0, (X_0, Y_0), in the phase plane must be found on an ellipse Γ, whose equation is

$$X_0^2+\frac{Y_0^2}{k^2}=|\mu|E_0^2 .$$

Similarly we have, on the right boundary,

$$\Psi(L)=|E_f|\cos\varphi', \quad \Psi'(L)=k|E_f|\sin\varphi' ,$$

where

$$E_f^+=\frac{|E_f|}{2}e^{-i\varphi'}, \quad E_f^-=\frac{|E_f|}{2}e^{i\varphi'} .$$

Note that, due to the continuity of Ψ and Ψ' across the boundaries, their above expressions at $x=0_-$ and $x=L_+$ (that is, outside the system) are the same as at $x=0_+$ and $x=L_-$ (inside the system).

Reasoning geometrically, we have to find an orbit solution connecting two points a_0, (X_0, Y_0), and a_f, (X_f, Y_f), located on the ellipse Γ such that $a_f=G^{(N)}a_0$ (see Fig. 9).

Assume now that $E_f^-=E_0e^{i\gamma}$: $\gamma=\varphi+\varphi'$ is the imposed phase shift between the two incident waves illuminating the system. It is easily seen that satisfying the zero-flux condition demands not only that $|E_f^-|=|E_0^+|$ but also that $\gamma=0$. Indeed the symmetry of the entire system with respect to its center implies that

$$\begin{bmatrix} E_f^+ \\ E_f^- \end{bmatrix}=\underline{A}\begin{bmatrix} E_0^+ \\ E_0^- \end{bmatrix} ,$$

where matrix $\underline{A}$ has the form

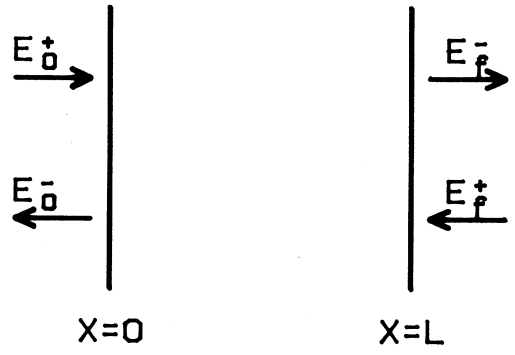

FIG. 8. Inward and outward fields on the boundaries of the system illuminated from both sides.

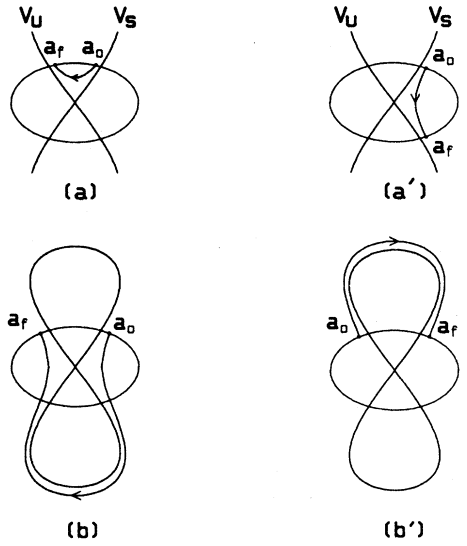

FIG. 9. The two types of solutions in a system illuminated from both sides. a_0 and a_f are the initial and final orbit points in the (X, Y) plane, located on ellipse Γ. V_u and V_s are the unstable and stable manifolds of the origin, respectively.

$$\underline{A}=\begin{bmatrix} a & i\mu \\ -i\mu & a^{*} \end{bmatrix} ,$$

μ being real, such that $|a|^2-\mu^2=1$. Then we have $E_0^-/E_0^+=(e^{i\gamma}+\mu)/a^{*}$. The zero-flux condition says that $|E_0^-/E_0^+|=1$, and therefore implies $\gamma=0$. As a result a_0 and a_f are symmetrical with respect to the Y axis. This ensures, due to the symmetry of the wave equation with respect to the sense of propagation of light, that the desired orbit solution (Λ) is itself symmetrical about the Y axis. a_0 and a_f are close to one of the intersections of Γ with V_s or V_u (the stable and unstable manifolds of the origin). Figure 9 shows that two types of solutions are expected.

(i) Orbits a and a' monotonically decrease from both edges up to the system center. These solutions, which we call "trivial," are analogous to those existing in a gap in the linear medium.

(ii) Orbits b and b' circling around the fixed points. They correspond to solitonlike solutions (multipeak solutions would be associated with several loops around the fixed points).

Λ is the unique solution (of type a or b) connecting a_0 and a_f through N iterations. In a real experiment where a stationary solution would be generated starting from given initial conditions, solutions of types a and b are in competition. We shall show in a subsequent paper that a precise procedure must be followed in order to observe the solitonlike solutions.

(2) Consider a system where the zero-flux condition is ensured thanks to a perfect mirror placed on one side. This system (illuminated from the other side) is dissym-

metric and an orbit solution satisfying the boundary conditions would connect an initial point a_0 on Γ to a point a_f located on the Y axis. In this case the solution is no longer unique since a_f is arbitrary on Y axis. This reflects the fact that one less boundary condition is imposed to the system, compared to the previous case. Here indeed the wave has a prescribed amplitude on one edge of the system, and it vanishes on the other one. Now remember that a_f is located in the near neighborhood of the unstable manifold of the origin, and its coordinates are very sensitive functions of the a_0 coordinates. Therefore we can expect those solutions to be dynamically unstable. Obviously this conclusion holds only for the solitonlike solution, and we expect to observe only the trivial one. We shall show (cf. the future paper) that numerical simulation of the time-dependent problem indeed confirms this conjecture.

The same kind of conclusions (and conjectures) hold for the other localized stationary solutions, namely they can be observed only in symmetrical systems.

A last point is the following. Consider again the solitonic case in a symmetric system, a prescribed topology (that is for a given number of loops around the fixed points), and a given size of the system (given value of N). Then there could be no stationary solution available. Suppose indeed that the incident fluxes are very small. Then ellipse Γ has a small extension and initial point a_0 lies very close to the origin; therefore many iterates of a_0 will be needed to "escape" from the origin neighborhood (the smaller the Floquet exponent or the modulation amplitude, the more iterates needed). But a solitonic solution must circle around fixed point F which is at a given distance (of the order of $\sqrt{\varepsilon}$ in the center of the gap) from the origin: this is impossible unless N is large enough. The condition obeyed by the incident flux in order to achieve a solitonlike solution can be estimated as follows: the largest Floquet exponent of the origin being given by $s=e^{\varepsilon\pi/4}$, the wave amplitude after N iterations is roughly given by $\Psi_0\sqrt{\mu}s^N$. We then obtain the condition

$$\Psi_0\sqrt{\mu}\gtrsim\sqrt{\varepsilon}e^{-N\varepsilon\pi/4} . \tag{22}$$

VI. CONCLUSION

It is interesting to compare the localized structures obtained in the present problem with those found in a linear system whose propagation constant is modulated with two incommensurate frequencies (see, for instance, Ref. 2). In this case the shape of the localized solutions is determined by the spatial structure of the refractive index field, and it exhibits the same symmetries. In the nonlinear problem, the global spatial homogeneity of the Floquet solutions (of the linearized equations) is broken by the nonlinear Kerr effect. But it is restored on the average (i.e., averaging over many successive peaks) by the stochasticity.

The localized structures which appear near the bifurcation of cycles with winding number $1/n$ ($n=1,2,3,4$) are "nearly analytic" solutions of the wave equation. Actually they are weakly chaotic and their stochastic character is responsible for their finite spatial extension. The onset of the stochasticity near a bifurcation appears numerically as a critical phenomenon, and it would deserve a theoretical study itself.

The temporal stability of the stationary solutions will be analyzed in the subsequent paper.

ACKNOWLEDGMENTS

We thank L. Macon, C. Montes, and D. Sornette for interesting discussions.

APPENDIX A: PERTURBATIVE ANALYSIS IN THE FIRST GAP ($k\approx1$) FIXED POINTS OF $G^{(2)}$

For convenience we rewrite the wave equation in the form

$$Dy+k^2[1+\varepsilon\cos(2x)](y+\eta y^3)=0 , \tag{A1}$$

where D is the second-order derivative operator. We shall use the following expansions:

$$y=\sqrt{\varepsilon}[y_1(x,x_1,x_2+\cdots)+\varepsilon y_2(x,\dots)+\varepsilon y_3(x,\dots)+\cdots] \quad (x_k=\varepsilon^k x) ,$$

$$k^2=1+\varepsilon\mu_1+\varepsilon^2\mu_2+\cdots ,$$

$$D=(\partial_x+\varepsilon\partial_{x_1}+\varepsilon\partial_{x_2}+\cdots)^2$$

$$=\partial_x^2+2\varepsilon\partial_{x_1}\partial_x+\varepsilon^2(\partial_{x_1}^2+2\partial_{x_2}\partial_x)+\cdots .$$

We first recall that the limits of the linear gap are given by

$$k^2=1\pm\varepsilon/2 .$$

At *first perturbative order* we have

$$(\partial_x^2+1)y_1=0 ,$$

whose solution reads

$$y_1=A(x_1,\dots)e^{ix}+A^*e^{-ix} . \tag{A2}$$

At *second perturbative order* we get

$$(\partial_x^2+1)y_2=-[2\partial_{x_1}\partial_x y_1+y_1\cos(2x)+\eta y_1^3+\mu_1 y_1] . \tag{A3}$$

The solvability conditions are

$$2i\partial_{x_1}A+(\mu_1+3\eta|A|^2)A+\frac{A^*}{2}=0 \tag{A4}$$

and the conjugate imaginary equation.

Let us determine the fixed points of $G^{(2)}$. They are periodic solutions of the wave equation with period 2π. Therefore A must be constant in expression (A2), which implies, at first order, that $\partial_{x_1}A=\partial_{x_1}A^*=0$. Setting $\beta=\mu_1+3\eta|A|^2$, the solvability conditions then imply $\beta=\pm\frac{1}{2}$.

Case $\beta=\frac{1}{2}$. The solvability conditions also imply

$$A^*=-A, \quad 3\eta|A|^2=\tfrac{1}{2}\varepsilon-\mu_1 . \tag{A5}$$

If $\eta=1$ this relation determines two periodic solutions

and therefore two fixed points of F_1 provided $\mu_1 < \frac{1}{2}$ (remember that $\mu_1 = \frac{1}{2}$ corresponds to the right edge of the first gap). If $\eta = -1$ the fixed points exist for $\mu_1 < -\frac{1}{2}$. According to (A5), A is pure imaginary and the periodic solution read, at first order,

$$y_{\mathrm{I}} = \pm[\tfrac{4}{3}\eta(1+\tfrac{1}{2}\varepsilon - k^2)]^{1/2}\sin(x) .$$

y_{I} provides two fixed points of $G^{(2)}$ located on the Y axis, symmetrical with respect to the origin.

Case $\beta = -\frac{1}{2}$. The solvability conditions yield, in the same way,

$$y_{\mathrm{II}} = \pm[\tfrac{4}{3}\eta(1-\tfrac{1}{2}\varepsilon - k^2)]^{1/2}\cos(x) .$$

y_{II} provides two fixed points of $G^{(2)}$ located on the X axis, symmetrical with respect to the origin. Putting $Z(x) = \sqrt{\varepsilon}\, A(\varepsilon x)$, we obtain the equations of the main text.

Linearizing Eq. (14) around the fixed point of $G^{(2)}$, we find that this point is stable (elliptic) if $\beta = -\frac{1}{2}$, and hyperbolic if $\beta = \frac{1}{2}$.

APPENDIX B: EQUATIONS FOR HETEROCLINIC ORBITS

We first make a perturbative expansion of the solution of the linearized wave equation near $k = 2$ (Floquet solution). This equation reads

$$Ly = 0$$

with

$$L = D + k_0^2[1 + \varepsilon\cos(2x)] , \tag{B1}$$

D being the second-order differential operator. The perturbative analysis is standard, and yields

$$y = A\Lambda + A^*\Lambda^*$$

with

$$\Lambda = e^{ik_1 x} + \frac{\varepsilon k_0^2}{8}\left[\frac{e^{i(k_1+2)x}}{1+k_0} + \frac{e^{i(k_1-2)x}}{1-k_0}\right] , \tag{B2}$$

where

$$k_1 = k_0\left[1 + \frac{k_0^2\varepsilon^2}{16(1-k_0^2)}\right] . \tag{B3}$$

Λ and Λ^* are the eigenvectors of the L operator associated with the zero eigenvalue. In the calculation of the fourth resonance we shall consider wave-number values k_0 such that $k_1 = \frac{1}{2}$. Now the nonlinear wave equation reads

$$Dy + k^2[1 + \varepsilon\cos(2x)](y + y^3) = 0 ,$$

and we use the following expansion in terms of the parameter α, characterizing the deviation of the wave number from the bifurcation value k_0:

$$y = \alpha y_1(x, x_1, x_2, \dots) + \alpha^3 y_2 + \cdots \quad (x_k = \alpha^k x) ,$$

$$k^2 = k_0^2 + \alpha^2\mu_1 + \alpha^4\mu_2 + \cdots ,$$

$$D = \partial_x^2 + 2\alpha^2\partial_{x_1}\partial_x + \alpha^4(\partial_{x_1}^2 + 2\partial_{x_2}\partial_x) + \cdots .$$

At first order we solve $Ly_1 = 0$ which gives $y_1 = A\Lambda + A^*\Lambda^*$.

At second order we must solve

$$-Ly_2 = 2\partial_{x_1}\partial_x y_1 + [1 + \varepsilon\cos(2x)](\mu_1 y_1 + k_0^2 y_1^3) . \tag{B4}$$

Now ξ and ξ^* belong to the kernel of L (since L is self-adjoint). Therefore the right-hand side of Eq. (B4) must be orthogonal to Λ and Λ^*. Using the above expressions for Λ and Λ^*, we obtain as a solvability condition (up to the first order in ε)

$$2ik_1\partial_{x_1} A + (3k_0^2|A|^2 + \mu_1)A + \delta_{k_1,1/2}(3\varepsilon/8)(A^*)^3 = 0 ,$$

where δ is the Kronecker delta. The last term of this equation is responsible for the fourth resonance. For $k_1 = \frac{1}{2}$, we obtain

$$i\partial_{x_1} A + (\tfrac{3}{4}|A|^2 + \mu_1)A + 3\varepsilon/8(A^*)^3 = 0 . \tag{B5}$$

Setting $A = \rho e^{i\theta}$, we find that the fixed points are given by

$$\theta = (k+1)\pi/4, \quad \rho^2 = -(4\mu_1/3)(1 \pm \varepsilon/2)^{-1} ,$$

and the parametric equations of the orbits, in the (ρ, θ) representation, are

$$d\rho/dx = (3\varepsilon/8)\rho^3\sin(4\theta) ,$$

$$d\theta/dx = \mu_1 + \tfrac{3}{4}[1 + (\varepsilon/2)\cos(4\theta)]\rho^2 .$$

We have the following invariant of the above equations:

$$C = \rho^2 + (3/8\mu_1)[1 + (\varepsilon/2)\cos(4\theta)]\rho^4 . \tag{B6}$$

(B6) is the equation of the orbits around the bifurcation point. The orbit containing the hyperbolic points corresponds to

$$C = (-4\mu_1/3)(1 + \varepsilon/2)^{-1} .$$

Finally, we come back to the (X, Y) plane by using

$$y = 2\alpha[A'\cos(x/2) - A''\sin(x/2)] ,$$

$$y' = -\alpha[A'\sin(x/2) + A''\cos(x/2)] ,$$

where A' and A'' are the real and the imaginary parts of A, respectively. To get the graph of $G^{(2)}$, we set $x = 2j\pi$ (j integer), and we obtain

$$X = 2\alpha A' ,$$

$$Y = -\alpha A'' .$$

In terms of X, Y variables the equations of the heteroclinic orbits read

$$X^2/4 + Y^2 \pm \sqrt{\varepsilon} XY = -4\mu_1\alpha^2/3 .$$

Setting $\lambda^2 = -\mu_1\alpha^2$ and $Z(x) = \lambda\Lambda(\lambda^2 x)$, we get the equations given in the main text.

[1] D. Mills and S. Trullinger, Phys. Rev. B **36**, 947 (1987).

[2] J. Peyraud and J. Coste, Phys. Rev. B **37**, 3979 (1988).